



Engaging dystonia networks with subthalamic stimulation

Konstantin Butenko^{a,1} , Clemens Neudorfer^{a,b} , Till A. Dembek^c , Barbara Hollunder^{d,e,f} , Garance M. Meyer^a , Ningfei Li^d , Simón Oxenford^d , Bahne H. Bahnert^{a,g,h} , Bassam Al-Fatly^d , Roxanne Lofredi^d , Evan M. Gordonⁱ , Nico U. F. Dosenbach^{ij,k} , Christos Ganos^l , Mark Hallett^m , Hyder A. Jinnahⁿ , Philip A. Starr^o , Jill L. Ostrem^p , Yiwen Wu^q , ChenCheng Zhang^r , Michael D. Fox^a , and Andreas Horn^{a,b,d,e}

Affiliations are included on p. 10.

Edited by Peter Strick, University of Pittsburgh Brain Institute, Pittsburgh, PA; received August 28, 2024; accepted December 2, 2024

Deep brain stimulation is an efficacious treatment for dystonia. While the internal pallidum serves as the primary target, recently, stimulation of the subthalamic nucleus (STN) has been investigated. However, optimal targeting within this structure and its surroundings have not been studied in depth. Indeed, historical targets that have been used for surgical treatment of dystonia are directly adjacent to the STN. Further, multiple types of dystonia exist, and outcomes are variable, suggesting that not all types would profit maximally from the same target. Therefore, a thorough investigation of neural substrates underlying stimulation effects on dystonia signs and symptoms is warranted. Here, we analyze a multicenter cohort of isolated dystonia patients with subthalamic implantations ($N = 58$) and relate their stimulation sites to improvements of appendicular and cervical symptoms as well as blepharospasm. Stimulation of the ventral oral posterior nucleus of thalamus and surrounding regions were associated with improvements in cervical dystonia, while stimulation of the dorsolateral STN was associated with improvements in limb dystonia and blepharospasm. This dissociation was matched by structural connectivity analysis, where the cerebellothalamic, corticospinal, and pallidosubthalamic tracts were associated with improvements of cervical dystonia, while hyperdirect and subthalamopallidal pathways with alleviation of limb dystonia and blepharospasm. On the level of functional networks, improvements of limb dystonia were associated with connectivity to the corresponding somatotopic regions in the primary motor cortex, while alleviation of cervical dystonia to the cingulo-opercular network. These findings shed light on the pathophysiology of dystonia and may guide DBS targeting and programming in the future.

deep brain stimulation | structural connectivity | sweet-spot analysis | cervical dystonia | limb dystonia

Building upon decade-long experience of ablative surgeries (1), in 1999, the first cases of deep brain stimulation (DBS) in the internal pallidum (GPi) were published (2, 3). Soon after, the GPi became an established DBS target for various types of dystonia (4), including clinical phenotypes with cervical, orofacial, and limb manifestations (5–7). Yet, while generally established, the treatment outcome is variable (8, 9), with stimulation sometimes being limited by side-effects such as gait impairment (10, 11), dysarthria, (12) and bradykinesia (13). More recently, the subthalamic nucleus (STN) has been investigated as an alternative target (14, 15) with clinical trials suggesting comparable efficacy (16, 17). Studies have extensively mapped optimal stimulation sites within the GPi (18, 19) and demonstrated that specific forms of dystonia may best respond to stimulation of specific circuits that may connect cortical, basal ganglia, thalamic, and cerebellar nodes (19). Such studies, however, have not been carried out based on stimulation data for the STN. Moreover, the STN occupies a unique anatomical location that is traversed by projections of various neural circuits and resides directly adjacent to multiple gray matter areas. Indeed, some of these structures, such as the fields of Forel (20) and various nuclei of the thalamus (21) have been targeted using electrical stimulation and ablations for treatment of dystonia in the past. It could well be the case that by activating dorsal contacts on electrodes that had been implanted with the STN in mind, one would serendipitously modulate adjacent structures, such as the subthalamic area or caudal zona incerta, thalamic nuclei, or the white matter bundles traversing this region, such as ansa and fasciculus lenticulares, comb fibers or cerebellothalamic tract (22). We hypothesize that, while the complex anatomy of this region may be challenging to identify specific target sites, it may also provide a powerful opportunity, since multiple sites and networks could be reached with a single electrode. In fact, once this region has been mapped in more detail, it could become possible to engage different circuits affected by dystonia pathophysiology (23), potentially in simultaneous fashion, by coactivating different contacts along the same electrode.

Significance

Deep brain stimulation is an effective treatment option for dystonia. While the internal pallidum is the standard target, more recently, the subthalamic nucleus has been targeted. We analyze a multicenter cohort of isolated dystonia patients with subthalamic implantations. We identify two distinct networks associated with optimal improvements of limb dystonia and blepharospasm vs. axial types of dystonia. The first primarily involves the basal ganglia circuitry and the primary motor cortex, while the second maps onto thalamic motor nuclei and is associated with a phylogenetically older motor system involving the cingulo-opercular network. These findings may shape our understanding of dystonia and could guide deep brain stimulation targeting and programming in the future.

Preprint server: A preprint of this manuscript was published at medRxiv.org under [Creative Commons Attribution-NonCommercial-NoDerivatives License 4.0 \(CC BY-NC-ND\)](https://creativecommons.org/licenses/by-nc-nd/4.0/), see <https://doi.org/10.1101/2024.05.24.24307896>.

Competing interest statement: R.L. reports personal fees from Medtronic. M.D.F. has intellectual property on the use of brain connectivity imaging to analyze lesions and guide brain stimulation, is a consultant for Magnus Medical, Soterix, Abbott, and Boston Scientific, and has received research funding from Neuronetics. A.H. reports lecture fees for Boston Scientific and is a consultant for FxNeuromodulation and Abbott. K.B., C.N., T.A.D., B.H., G.M.M., N.L., S.O., B.H.B., B.A.-F., E.M.G., N.U.F.D., C.G., M.H., H.A.J., P.A.S., J.L.O., Y.W., and C.Z. declare no competing interests.

This article is a PNAS Direct Submission.

Copyright © 2025 the Author(s). Published by PNAS. This article is distributed under [Creative Commons Attribution-NonCommercial-NoDerivatives License 4.0 \(CC BY-NC-ND\)](https://creativecommons.org/licenses/by-nc-nd/4.0/).

¹To whom correspondence may be addressed. Email: konstantinmgtu@gmail.com.

This article contains supporting information online at <https://www.pnas.org/lookup/suppl/doi:10.1073/pnas.2417617122/-DCSupplemental>.

Published January 8, 2025.

Here, we retrospectively investigate optimal targets, tracts, and networks based on a comparably large multicenter cohort with heterogeneous dystonic symptoms. We employ previously introduced statistical tools for local mapping as well as structural and functional connectivity analyses (24). We focus on three clusters of dystonia signs and symptoms that were motivated by both clinical experience and literature findings from historical (21) as well as modern times (19, 25, 26). Namely, we cluster the available cohort into three partly overlapping subcohorts that presented with predominant baseline symptoms of cervical dystonia, appendicular/limb dystonia (extremities), or blepharospasm (periocular region). By applying the multimodal neuroimaging analysis, we are able to investigate similarities and differences for optimal targeting in STN-DBS for these three phenotypes of dystonia on local, tract, and network levels.

Materials and Methods

Patient Cohorts and Imaging. To identify anatomical substrates associated with optimal clinical outcomes, we aggregated a total of 78 patients across two independent centers (Shanghai $N = 65$, San Francisco $N = 13$) who underwent bilateral STN-DBS for treatment of isolated therapy-refractory dystonia, which is the largest STN-DBS dystonia dataset studied, to date. Clinical results of these cases have been published elsewhere (27–29). This study was conducted in accordance with ethical standards and approved by the Institutional Review Board of the Brigham and Women's Hospital and Harvard Medical School, Boston, Massachusetts (protocol #2022P000736). Given the secondary use of research data, the study was exempted from obtaining informed consent. The STN targeting strategy was not dependent on clinical phenotype. Ages of onset, disease durations, and symptom distributions varied across subjects (see Fig. 1 and *SI Appendix, Table S1* and *Dataset S1* for inclusion criteria and demographics). All patients were stimulated in the voltage-controlled mode using Medtronic (Minneapolis, MN), SceneRay (Suzhou, China), or PINS (Beijing, China) DBS systems employing four contact electrodes with either 0.5 or 1.5 mm spacing. Due to the significant difference in N , we refrained from comparative subanalyses between cohorts and further addressed the entire dataset. Based on pathophysiological considerations from prior research (5, 19, 25, 30–34) and clinical experience, patients were grouped according to their baseline Burke-Fahn-Marsden Dystonia Rating Scale (BFMDRS) scores. Due to complex and heterogeneous manifestations of dystonia, we deliberately avoided classifying patients exclusively, but assigned them to the groups in overlapping fashion. Fig. 1 graphically illustrates the grouping and summarizes inclusion criteria for each group. *SI Appendix, Fig. S1* shows the covariance structure of improvements across motor symptoms. We then analyzed clinical improvements of cervical (neck), appendicular (arms and legs) as well as blepharospasm (eyes) items of the BFMDRS assessed after at least three months of DBS (5) (mean and SD: 15.6 ± 14.4 , range: 3 to 84 mo). Refer to *SI Appendix, Table S1* and *Dataset S1* for details.

For every patient, electrode localizations and stimulation volumes were computed using Lead-DBS v3.0 (24) described in detail elsewhere (22). Briefly, preoperative MRI and postoperative CT/MRI images were first coregistered and then nonlinearly warped to ICBM 2009b Nonlinear Asymmetric ("MNI") space using advanced normalization tools (ANTs, <https://stnava.github.io/ANTs/>). Postoperative coregistrations were additionally corrected for brain shift due to possible pneumocephalus (35). The nonlinear warps were manually refined in the STN region using the WarpDrive tool (36) in case the automatic delineation of the nucleus was visibly off. Next, the electrode trajectories were reconstructed using either PaCER (37) or TRAC/CORE (38) algorithms for postoperative CT ($N = 59$) and MRI scans ($N = 11$), respectively (Figs. 2–4, panel A). Finally, based on clinical stimulation protocols and electrode localizations, distributions of the induced electric fields were computed using the SimBio/FieldTrip pipeline (<https://www.mrt.uni-jena.de/simbio/>; <http://fieldtriptoolbox.org/>) (39) to solve the static formulation of Maxwell's equations using the Finite Element Method. The computational domain was discretized into four compartments with distinct electrical conductivities (metal: 10^8 S/m; insulation: 10^{-16} S/m; gray matter: 0.33 S/m; white matter: 0.14 S/m) according to the electrode reconstruction and the basal ganglia tissue distribution defined by the DISTAL

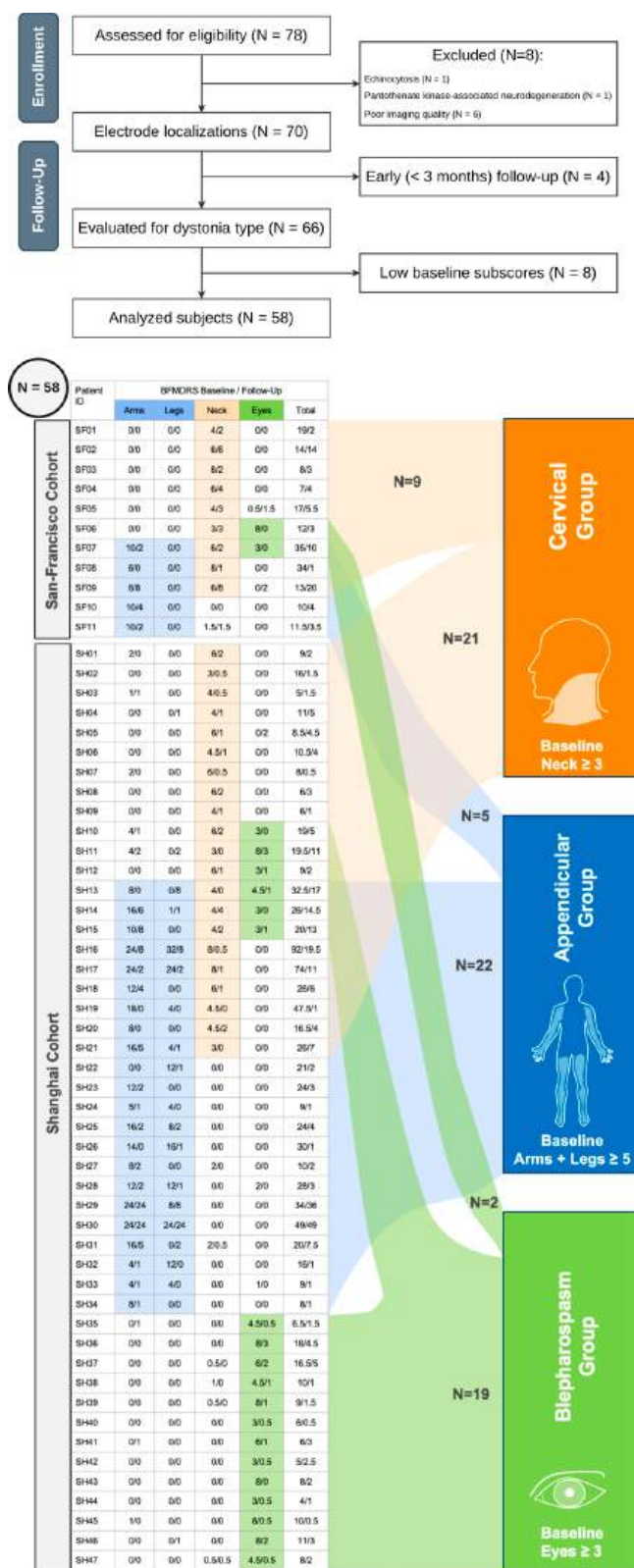


Fig. 1. Clinical characteristics and subdivision of patients into three overlapping subcohorts. (Upper Panel) Consort flowchart for inclusion criteria. Patients from two independent cohorts (Shanghai $N = 65$, San Francisco $N = 13$) were considered as a single dataset. The final dataset consisted of 58 subjects. (Lower Panel) Classification into dystonic groups based on corresponding baseline subscores. Note that the patients are assigned to groups in nonexclusive fashion.

atlas (40, 41). The spatial distribution of the electric field magnitude (further referred to as E-field) was subsequently used as the main underlying parameter for the stimulation effect.

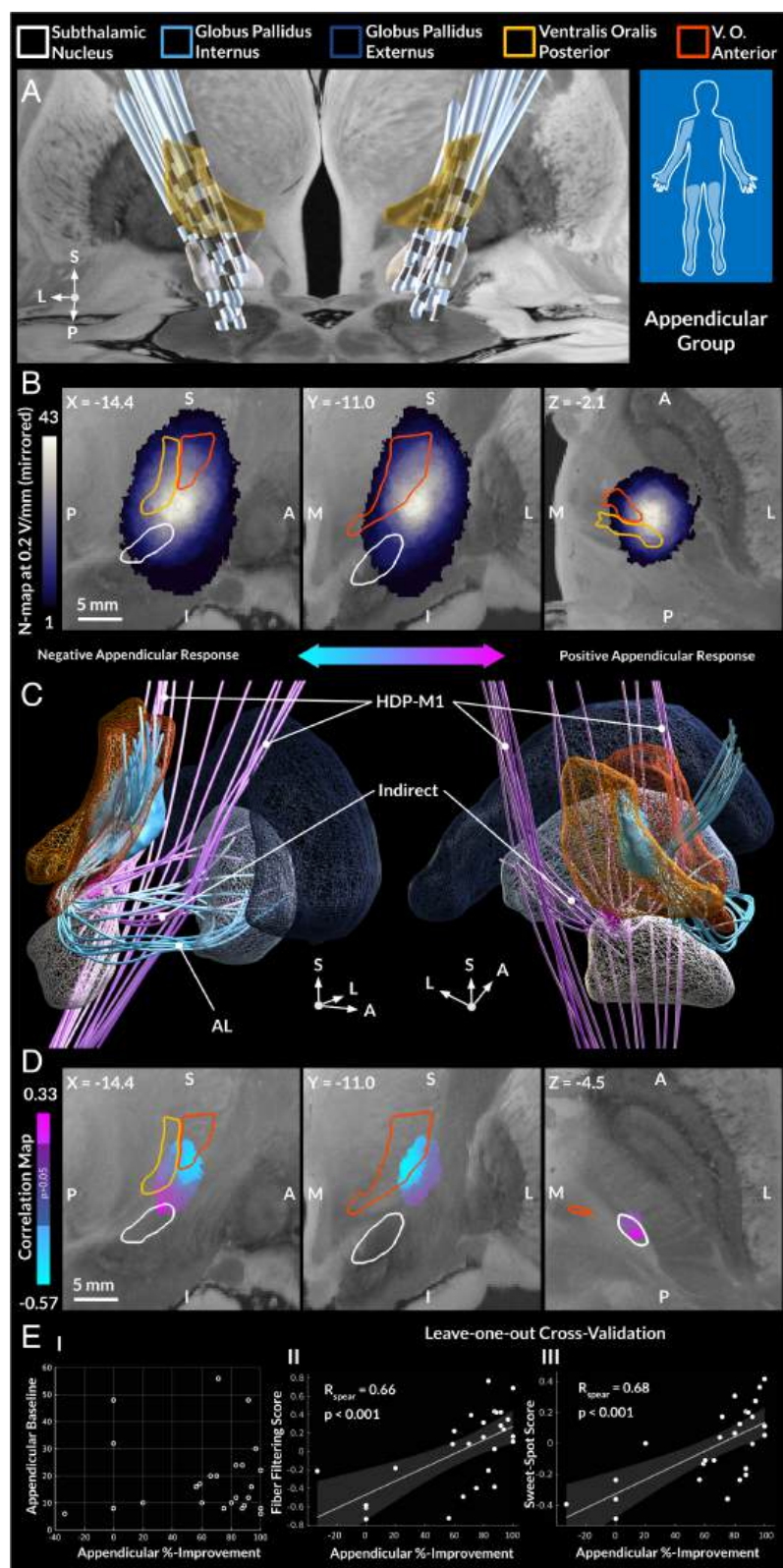


Fig. 2. Appendicular dystonia. (A) Electrode reconstructions for patients included in the appendicular group. Note that proximal electrode contacts and stimulation volumes covered the ventral thalamus due to a comparably large contact spacing in the implanted electrodes. (B) Distribution of stimulation volumes, defined by electric fields thresholded at the magnitude of 0.2 V/mm. The peak intensity resides in the white matter region dorsolateral to the STN. (C) Structural connectivity statistically associated ($P < 0.05$) with appendicular improvement under DBS. Stimulation of the subthalampallidal (indirect) pathway and the hyperdirect projections from the lower and upper extremity regions of the primary motor cortex (HDP-M1) positively correlated with clinical improvements, while the opposite was observed for the AL. (D) Voxel-wise correlation map of the electric field magnitude with stimulation outcome. The sweet-spot, thresholded for significance, localized to the dorsolateral aspect of STN, while the sour-spot predominantly resided in the ventral oral anterior nucleus of thalamus. (E) Clinical scores and their association with the fiber filtering and sweet-spot scores, quantified by spatial correlations between E-field distributions and sweet-spots/tractograms; Fisher Z-transformation was applied to the sweet-spot scores. To indicate robustness of the association, leave-one-out cross-validation is reported. For 10-fold cross-validations, see *SI Appendix, Fig. S6*. Models were also subjected to permutation tests: $R = 0.69$, $P < 0.001$ and $R = 0.79$, $P < 0.001$ for the sweet-spot and fiber filtering models, respectively.

Analysis of Neural Correlates. Since DBS affects not only gray but also white matter and distributed brain networks (42–44), optimal DBS targets may best be defined in a form of a triad that consists of i) the specific location associated with optimal outcomes (sweet-spot), ii) the spatial trajectory of white matter tracts associated with optimal outcomes, and iii) the polysynaptic functional brain network associated with optimal outcomes (45). Therefore, we analyzed optimal target sites for each type of dystonia on a local, tract- and network level. To do so, we carried out DBS sweet-spot, fiber filtering, and network mapping analyses, respectively. These methods have been standardized in Lead-DBS (19, 22, 46–48).

In brief, these approaches involve mass-univariate correlation analyses based on the voxel-wise [sweet-spot (19, 48)] and fiber-wise [fiber filtering (19, 22, 47)] E-field metric as well as fMRI-based correlation maps [network mapping (19, 47)]. For the fiber filtering analysis, relevant streamlines were identified from tracts implemented in the Basal Ganglia Pathway Atlas (49). Created by experienced neuroanatomists in semimanual fashion, this atlas precisely describes the majority of tracts directly affected by stimulation in the STN region. For network mapping, correlation maps were obtained based on an $N = 1,000$ normative resting state functional connectome (50, 51), seeded from each E-field to calculate

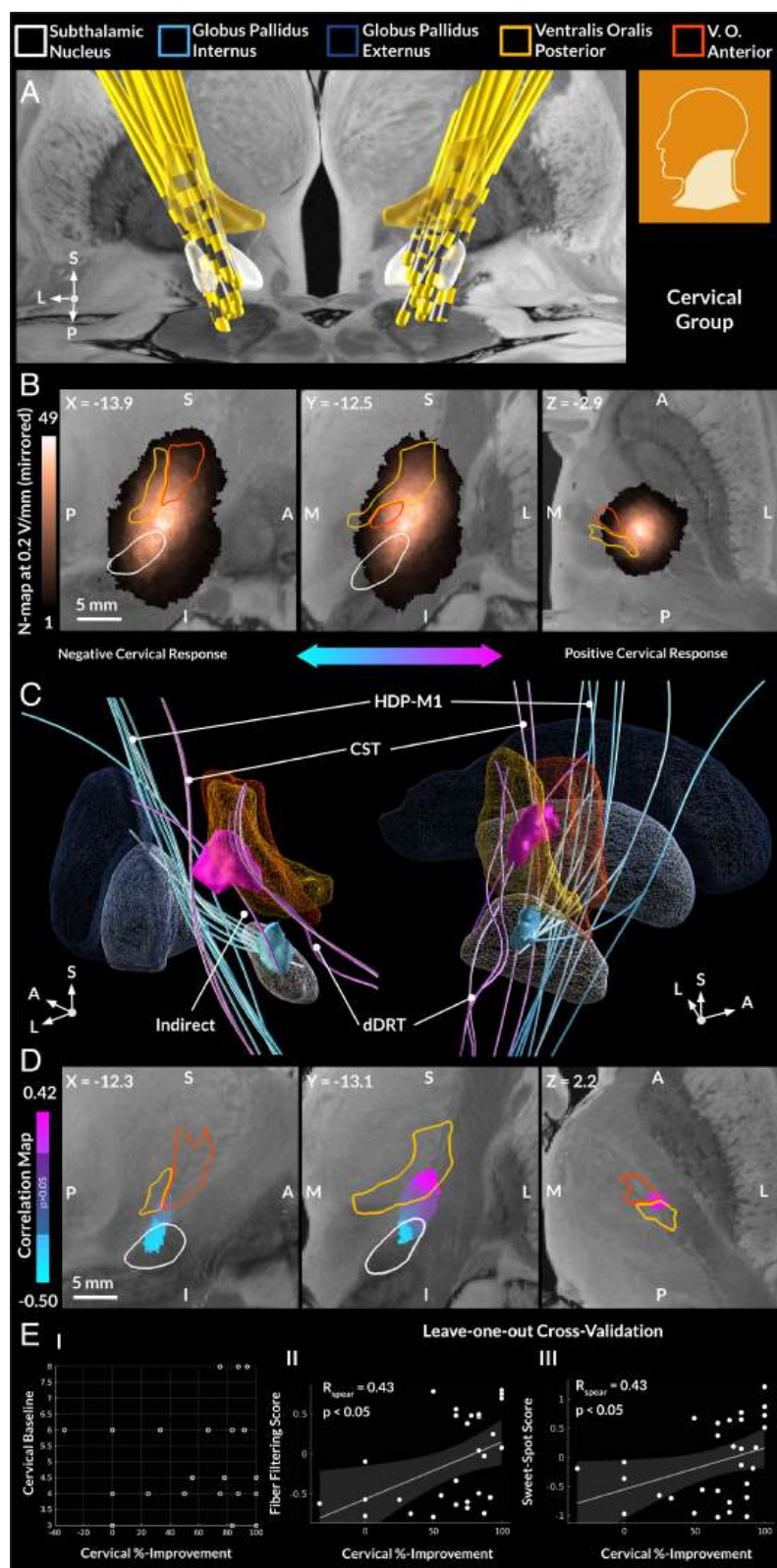


Fig. 3. Cervical dystonia. (A) Electrode reconstructions for patients included in the cervical group. Note that proximal electrode contacts and stimulation volumes covered the ventral thalamus due to a comparably large contact spacing in the implanted electrodes. (B) Distribution of stimulation volumes, defined by electric fields thresholded at the magnitude of 0.2 V/mm. The peak intensity resides in the white matter region dorsolateral to the STN. (C) Structural connectivity statistically associated ($P < 0.05$) with cervical improvement under DBS. Stimulation of the cerebellothalamic (dDRT) and corticospinal tracts (CST), as well as subthalamic afferents from the globus pallidus externus (indirect) positively correlated with clinical improvements, while the opposite was observed for the hyperdirect pathway from the primary motor cortex (HDP-M1). (D) Voxel-wise correlation map of the electric field magnitude with stimulation outcome. The sweet-spot, thresholded for significance, primarily localized to the ventral oral posterior nucleus of thalamus, while the sour-spot was identified in the central STN. (E) Clinical scores and their association with the fiber filtering and sweet-spot scores, quantified by spatial correlations between E-field distributions and sweet-spots/tractograms; Fisher Z-transformation was applied to the sweet-spot scores. To indicate robustness of the association, leave-one-out cross-validation is reported. For 10-fold cross-validations, see *SI Appendix, Fig. S6*. Models were also subjected to permutation tests: $R = 0.50$, $P = 0.055$ and $R = 0.62$, $P < 0.05$ for the sweet-spot and fiber filtering models, respectively.

respective connectivity maps (52). Note that all analyses employed Spearman's correlations due to the nonnormal distributions of both E-fields and clinical scores (for the latter, see Figs. 2–4, panel E). The workflow of the applied methodology is described in *SI Appendix*. Since clinical improvements were evaluated for bilateral stimulations, we followed previous retrospective studies on dystonia and assumed that the mirrored stimulation would produce the same clinical effect on the scores pulled across the hemibodies (18, 19). This allowed us to mirror the stimulation sites across the two hemispheres when defining the models.

Such analyses are conducted in a highly multidimensional (voxel or fiber) space that is prone to overfitting. Therefore, to evaluate robustness of generated models, we subjected them to leave-one-out (LOO) and 10-fold cross-validations. Here, in each iteration, a part of the data were held-out, and the model was recalculated only based on the remaining subjects. Scores for the held-out patients were computed based on this model, and the procedure was repeated across all folds/patients. The obtained scores were then correlated with the observed clinical improvement. For the 10-fold cross-validation, we repeated the procedure 10

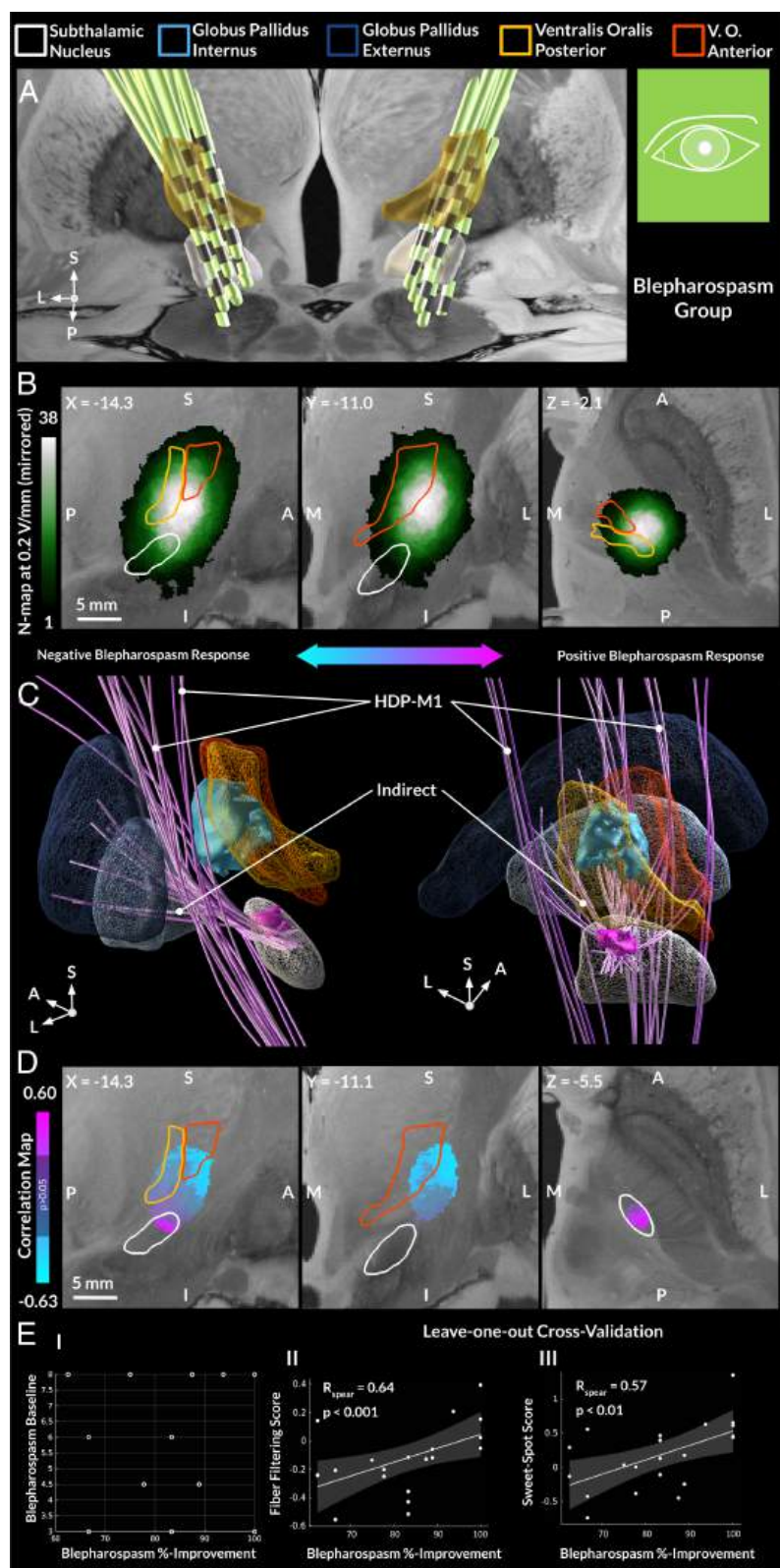


Fig. 4. Blepharospasm. (A) Electrode reconstructions for patients included in the blepharospasm group. Note that proximal electrode contacts and stimulation volumes covered the ventral thalamus due to a comparably large contact spacing in the implanted electrodes. (B) Distribution of stimulation volumes, defined by electric fields thresholded at the magnitude of 0.2 V/mm. The peak intensity resided in the white matter region dorsolateral to the STN. (C) Structural connectivity statistically associated ($P < 0.05$) with blepharospasm improvement under DBS. Stimulation of the subthalamopallidal tract (indirect), as well as the hyperdirect pathway from the primary motor cortex (HDP-M1) positively correlated with clinical improvements. (D) Voxel-wise correlation map of the electric field magnitude with stimulation outcome. The sweet-spot primarily localized to the STN proper, while the sour-spot resided in the capsule and, partially, in the ventral oral nuclei of the thalamus. (E) Clinical scores and their association with the fiber filtering and sweet-spot scores, quantified by spatial correlations between E-field distributions and sweet-spots/tractograms; Fisher Z-transformation was applied to the sweet-spot scores. To indicate the robustness of the association, leave-one-out cross-validation is reported. For 10-fold cross-validations, see *SI Appendix, Fig. S6*. Models were also subjected to permutation tests: $R = 0.73$, $P < 0.001$ and $R = 0.60$, $P < 0.01$ for the sweet-spot and fiber filtering models, respectively.

times (i.e., 100 models were generated in total) to ensure robustness for different configurations of folds (in the LOO case, naturally, only one configuration is possible). To quantify the possibility of a type I error, we also subjected models to permutation-based testing. Clinical improvement scores were permuted across patients 1,000 times to create a null distribution of models, to which the unpermuted model was compared. The null hypothesis was then rejected with a probability estimated by performance of the original model (quantified by the correlation coefficient) against the permuted models ($\alpha = 0.05$). Along the

same lines, we evaluated a similarity of sweet-spot maps comparing their correlation coefficient with correlations between the maps of permuted models.

Results

Out of 78 patients, two subjects were excluded due to a diagnosis of echinocytosis or pantothenate kinase-associated neurodegeneration, respectively. Six subjects were further excluded due to

missing or low-quality imaging data. For four subjects, only early (less than three months) follow-ups were available. Eight subjects had low baseline scores in all of the considered groups and were a priori excluded to avoid bias when analyzing percent improvements. Specifically, the bimodal baseline distributions (reflecting the difference in dystonia types) and underinformativeness of percent improvements (due to the low baseline) motivated the application of the minimal baseline thresholds. Additionally, to analyze whether these thresholds had qualitative effects, we conducted sweet-spot analyses using a -1 to $+1$ range of the thresholds (4 to 6 points for limb, 2 to 4 points for cervical and blepharospasm groups), which did not qualitatively alter results (SI Appendix, Figs. S2–S4). The consort flowchart in Fig. 1 summarizes these exclusions.

A total of 58 subjects were retained (29 female, mean age at surgery 40.2 ± 20.1 y, disease duration 6.6 ± 7.6 y, follow-up assessment 1.3 ± 1.2 y after surgery), who were nonexclusively assigned to the appendicular ($N = 27$), cervical ($N = 30$), and blepharospasm ($N = 21$) groups. For demographics and clinical results, see Fig. 1 and SI Appendix, Table S1, for individual scores and demographic data for all patients see Dataset S1. Four patients qualified for inclusion in all three groups, eight into both cervical and appendicular groups and four into cervical and blepharospasm groups. Across subjects, considerable variability in outcomes was observed in the total BFMDRS percent improvement ($67.7 \pm 28.4\%$) and body region-specific percent improvement (appendicular $73.7 \pm 32.1\%$, cervical $64.4 \pm 34.9\%$). Notably, the variance in clinical outcomes was comparably smaller in the blepharospasm group with patients showing a high response ($82.3 \pm 13.1\%$). Neither duration of the disease nor age at surgery significantly correlated with clinical outcomes for any of the considered groups, see SI Appendix, Fig. S5. Electrodes were localized to the region of the subthalamic nucleus in all patients as can be seen in panel A of Figs. 2–4. Across the three groups, the distribution of E-fields, binarized at 0.2 V/mm, clearly revealed the highest overlap in the region dorsolateral to the STN, see panel B in Figs. 2–4. In other words, even though the STN was the surgical target in these patients and electrodes were localized in the STN or in close proximity to the STN, in many patients, chronic stimulation was carried out by activating proximal contacts that resided in dorsally adjacent brain structures.

Appendicular Dystonia. For the appendicular group, the “sweet-spot” resided in the dorsolateral part of the STN, while the “sour-spot”, corresponding to suboptimal improvement, resided predominantly in the ventral oral anterior nucleus (V.o.a.) of thalamus bordering the internal capsule (Figs. 2D and 5). These results were robust when subjected to leave-one-out cross-validation (LOO: $R = 0.68$, $P < 0.001$, Fig. 2 E—III), 10-fold cross-validation (SI Appendix, Fig. S6), and permutation-based analysis ($R = 0.69$, $P < 0.001$). Notably, the sweet-spot corresponded to the terminating region of the hyperdirect pathway originating from the primary motor cortex (M1, Fig. 2C), whose stimulation was also associated with symptom improvements (LOO: $R = 0.66$, $P < 0.001$, Fig. 2 E—II; perm. test: $R = 0.79$, $P < 0.001$; for 10-fold see SI Appendix, Fig. S6). On the other hand, fibers associated with suboptimal improvements belonged to the ansa lenticularis (AL), which accordingly also traversed the sour-spot in V.o.a. Finally, on a polysynaptic network level, the functional connectivity analysis demonstrated a correlation of improvements with stronger connectivity to the precentral gyrus (Fig. 6). When repeating this analysis focusing on upper and lower limb items separately, mappings matched the ‘effector sites’ (i.e., arm and leg regions; Fig. 6C).

Cervical Dystonia. In contrast to the appendicular group, improvement of cervical dystonia primarily mapped to the ventral oral posterior nucleus (V.o.p.) of the thalamus, which has been described by Hassler as cerebellar receiving (53), and by Jones as pallidal receiving (54, 55) (Figs. 3D and 5; LOO: $R = 0.43$, $P < 0.05$, Fig. 3 E—III; perm. test: $R = 0.50$, $P = 0.055$; for 10-fold see SI Appendix, Fig. S6). Curiously, the sour-spot was identified in the central STN. DBS fiber filtering revealed a greater improvement with stimulation of the cerebellothalamic pathway (Fig. 3C), as well as the CST and a portion of the subthalamic afferents originating from the globus pallidus externus (LOO: $R = 0.43$, $P < 0.05$, Fig. 3 E—II; perm. test: $R = 0.62$, $P < 0.05$; for 10-fold see SI Appendix, Fig. S6). On the level of polysynaptic functional networks, higher improvements were associated with stronger connectivity to the cingulo-opercular network (56) (Fig. 6), but not the primary motor cortex, as in the case of appendicular dystonia. A secondary analysis, which repeated the same steps for a more inclusive axial improvement (comprising cervical, truncal, and oral improvements), revealed highly similar results, see SI Appendix, Fig. S7.

Blepharospasm. For blepharospasm signs, a generally strong response to DBS treatment was observed, see Fig. 4 E—I. The overall pattern of structures implied in symptom modulation was similar to the appendicular group (Figs. 4D and 5, permutation-based similarity $R = 0.58$, $P < 0.001$). Namely, sweet-spot mapping identified greater improvement of symptoms in the dorsolateral STN (LOO: $R = 0.57$, $P < 0.01$, Fig. 4 E—III; perm. test: $R = 0.73$, $P < 0.001$; for 10-fold see SI Appendix, Fig. S6), which also matched the termination site for the positively correlated fibers (Fig. 4C) of the hyperdirect pathway originating in M1 and the motor subthalamopallidal tract (LOO: $R = 0.64$, $P < 0.001$, Fig. 4 E—II; perm. test: $R = 0.60$, $P < 0.01$; for 10-fold see SI Appendix, Fig. S6). Relatively suboptimal results mapped to the internal capsule and partially to the V.o.a nucleus of the thalamus. For association of blepharospasm improvement with the sweet-spot and fibers of the appendicular group and vice versa, see SI Appendix, Fig. S8.

Discussion

The following conclusions may be drawn from this study. First, on a localized target level, different forms of dystonia seemed to best respond when modulating different stimulation sites, such as the subthalamic nucleus proper (appendicular dystonia and blepharospasm) or motor nuclei of the thalamus (axial forms of dystonia such as cervical or truncal dystonia). Second, on a tract level, stimulation of the STN circuitry was associated with improvements in appendicular dystonia, while cerebellothalamic fibers with axial dystonia. Third, on a polysynaptic network level, the former mapped to somatotopically plausible regions of the precentral motor homunculus, while the latter mapped to the agranular prefrontal cortex, which includes the cingulate motor area.

Symptom-Specific Network Modulation in Dystonia. Mappings of DBS effects across the three groups of dystonic symptoms may be insightful to understand the pathophysiology of dystonia, but also informative for clinical care. Both local mapping and structural connectivity analyses showed that modulation of the STN circuitry was beneficial for appendicular symptoms and blepharospasm, while improvement of axial (cervical) symptoms was observed for stimulation in the thalamic region. Prior literature findings may help to understand this dichotomy. While the basal ganglia have been considered a primary source of the dystonic

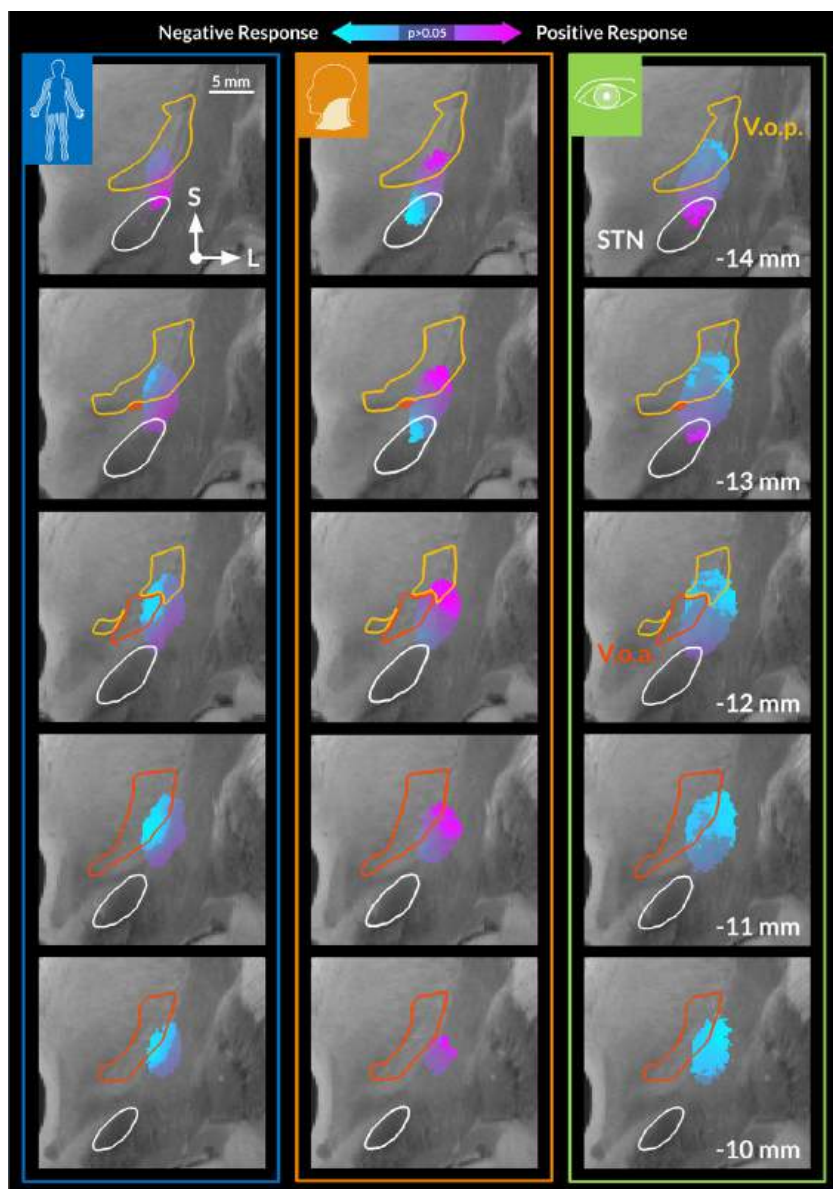


Fig. 5. Sweet-spot mappings in the three types of dystonia. The sweet- and sour-spots are computed by correlating distributions of electric fields with clinical outcomes across patients, coronal view. Note a partial inversion of the map for the cervical group, with the optimal stimulation site located in the thalamic and dorsal white matter region. A permutation-based similarity testing indicated a significant positive correlation of the appendicular and blepharospasm maps ($R = 0.58$, $P < 0.001$), and their nonsignificant negative correlation with the cervical map ($R = -0.09$, $P = 0.77$ and $R = -0.37$, $P = 0.11$, respectively).

pathophysiology (57–59), there is also evidence that demonstrates the involvement of the thalamus, brainstem, and cerebellum (32, 59, 60). Crucially, stimulation in and around the STN allows a direct engagement of the aforementioned brain regions via structural connectivity. For example, apart from the basal ganglia circuitry, STN-DBS may recruit thalamic afferents, such as pallidothalamic and cerebellothalamic tracts (61–63). Moreover, the differential mapping of dystonic phenotypes has in part been reported in prior studies. Namely, secondary limb dystonia has been linked to incidental basal ganglia lesions (25, 33). For secondary blepharospasm, a preferential lesion localization was not observed (25, 64). However, both pallidal and subthalamic targets were shown to be effective in Meige syndrome (65, 66), and for the latter, better outcomes were associated with stimulation in the dorsolateral STN (67), matching our findings. Secondary cervical dystonia has been associated with brainstem and cerebellar lesions (25, 31, 34) and management of cervical symptoms has been linked to surgical lesioning of pallidothalamic tracts in Forel's field H1 (68) and stimulation of this region (20). Similarly, optimal stimulation sites dorsal to the STN, including the zona incerta and Forel's field H2, have been reported in a recent STN-DBS study for cervical dystonia (69). Moreover, and in agreement with

our results, the cervical phenotype has been linked to abnormal functional connectivity in the executive control and primary visual networks (70), whose activity was modulated during sensory tricks (71). In seeming contrast to our results, secondary hand dystonia has been observed after thalamic lesions (25, 72–74), while its surgical lesioning was shown to be effective for treatment of writer's cramp and musician dystonia (75–77). However, as the thalamus receives both cerebellar and basal ganglia projections, it is unclear whether these lesions would rather fall into the basal ganglia, cerebellar, or mixed circuitry.

The structural connectivity analysis for cervical dystonia emphasizes cerebellothalamic projections. The role of the cerebellum is not surprising, when considering dystonia as a disorder that involves sensory components (23). Furthermore, abnormal cerebellar activation in fMRI was previously reported in patients with cervical dystonia (78). It is important, however, to emphasize the anatomical complexity of the region that we identify as the optimal stimulation site for this manifestation. The intricate trajectory of white matter tracts in the fields of Forel and zona incerta might not be comprehensively accounted for in our analysis. For example, in the employed normative pathway atlas (49), the pallidothalamic tracts traverse V.o.a. and terminate in the nucleus lateropolaris

thalami (Lpo), as delineated by the DISTAL Atlas (40, 41). On the other hand, pallidal projections were also reported for the V.o.p. region (55, 79), which overlaps with the optimal stimulation site found in our study. Furthermore, prior literature reports the involvement of the pallidothalamic tracts in the modulation of cervical symptoms (68, 80–83). Hence, an exclusive association of the therapeutic effect with either cerebellothalamic or pallidothalamic projections remains disputable. Regardless of this ambiguity, the present results as well as previous studies emphasize the role of the white matter region superior to the STN for alleviation of axial and cervical symptoms.

Insights Into Polysynaptic Motor Networks. By broadly grouping forms into appendicular vs. axial dystonia, our results mapped to two distinct networks that were either centered around the precentral homunculus or the agranular prefrontal cortex that involves cingulate motor areas (CMA). To interpret these results, a brief treatise that sets these findings into context with the phylogenetic development of the motor system appears helpful, which we attempt, in the following.

Phylogenetically, the “pyramidal” motor system of the precentral motor homunculus developed later and on top of an older “extrapyramidal” motor system that consisted of ventromedial and dorsolateral brainstem pathways projecting via rubrospinal, reticulo-/tecto-/vestibulospinal pathways to the ventro- and dorsomedial intermediate zones of the spinal cord (84, 85). As late as the lineage of primates, within the pyramidal motor system and CST, a corticomotoneuronal system (CM) evolved, which allowed cortical layer V motor neurons direct access to spinal motor neurons, bypassing tectal and other brainstem relays (85). The CST and even more so, the CM system are predominantly used for fine motor control, such as skilled hand and digit movements required

for tool use in primates (85). At the same time, the phylogenetically older motor systems that synapse in midbrain and brainstem regions during their descending course [groups “A and B” in the influential categorization by Hans Kuypers (84)] are involved in more “axial” motor control, such as postural control of the head, neck, and trunk, as well as proximal limb movements (85).

While cortical projections to the newer system predominantly reside in M1, the ones projecting to the “older” system also include strong projections from regions in the agranular prefrontal cortex, which includes the CMA (86). The agranular PFC was among the earliest cortical regions to develop in early mammals and is considered the prototype of “motor” cortex (87). Indeed, the fMRI map involved in axial symptom improvements of dystonia bears strong resemblance with the agranular cortex as well as with functional connectivity seeded from extrapyramidal motor regions such as the red nucleus (Fig. 6D). Recently, this functional network has been termed “cingulo-opercular network” (CON) and was investigated using precision functional mapping based on fMRI (26, 56, 88). Corresponding to anatomical knowledge, the CON, which has also been referred to as the “action mode network” (56), seems to be involved in cognitive, observational, and somatomotor domains, with the latter being functionally expressed centrally, precisely where anatomical textbook knowledge locates the CMA (87). As M1, this region contains a population of layer V gigantopyramidal neurons which project to the intermediate zone of the spinal cord (87), i.e., is part of Kuypers’ group A system responsible for head, neck, trunk, and proximal limb movements (3). It is reciprocally connected with primary motor cortex (87) and functionally connected to phylogenetically older parts of M1, which have recently been described as the somatocognitive action network (SCAN) (26). This latter network has similarly been associated with coarse and

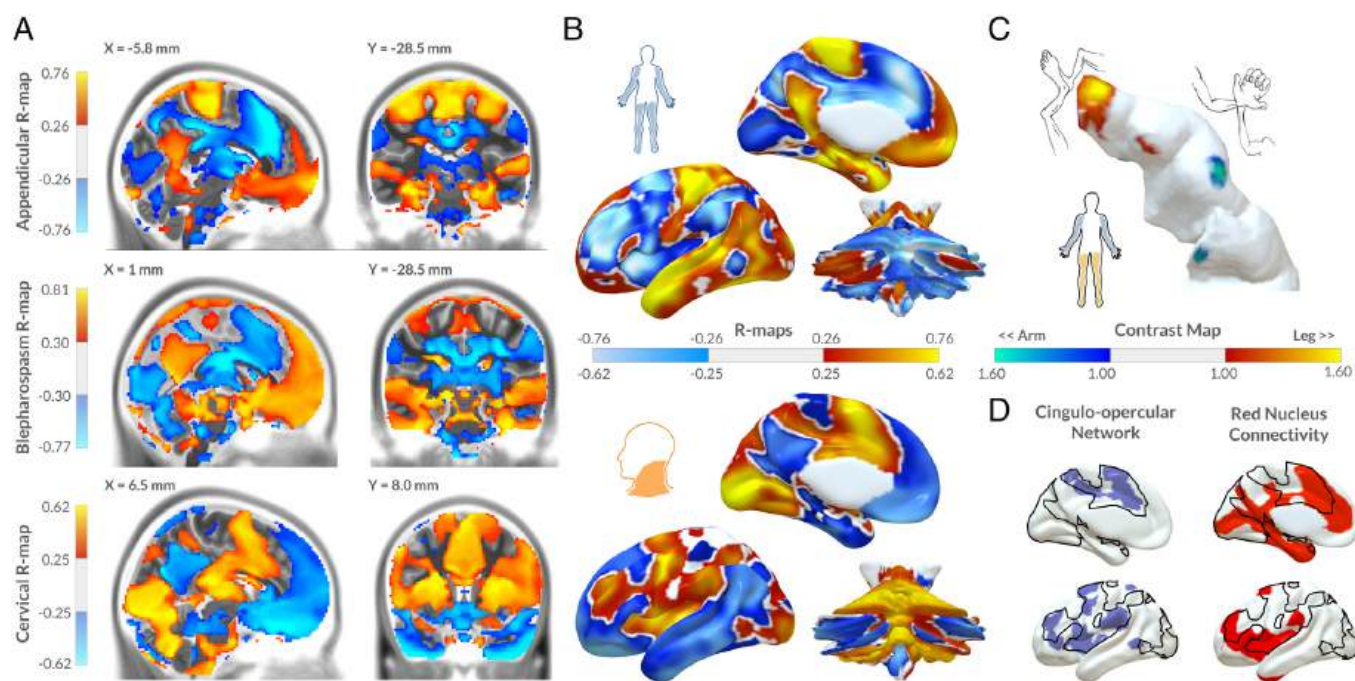


Fig. 6. Functional connectivity patterns associated with improvements in the three types of dystonia. (A) Maps of symptomatic improvement-associated functional connectivity across groups thresholded at the uncorrected significance level $P < 0.05$. (B) Surface projections of maps for appendicular (Top) and cervical (Bottom) improvement. While the appendicular improvement mapped onto a network that included peaks in the primary motor cortex, the cervical improvement map overlapped with the phylogenetically older motor system within the agranular prefrontal cortex and the cingulate motor area. Functionally, this network resembles the cingulo-opercular network (56) and connectivity profiles seeded from extrapyramidal motor areas such as the red nucleus (see panel D). (C) Contrast map of leg versus arm improvement (difference of z-scored symptomatic improvement maps) projected onto the primary motor cortex. This map peaked at the leg area (for lower limb improvements) and the hand knob (for upper limb improvements). The homuncular regions are adapted from ref. 26 (licensed under CC-BY 4.0). (D) Cingulo-opercular network (56) and functional connectivity map of the red nucleus bear resemblance to the cervical improvement map (black outlines and see panel B).

stereotypical axial body movements (26) and should be seen as standing in contrast to the aforementioned homuncular parts of M1 that are involved in fine motor control of distal limbs. Both CON (specifically, its cingulate motor domains) and SCAN (in M1) could be seen as collaborating partners in a phylogenetically older motor network that is involved in broader, axial body and proximal limb movements (26). Indeed, functional connectivity of DBS electrodes to both CON and SCAN networks have recently been implied with treatment success in other motor disorders such as Parkinson's Disease (89) and Tourette's Syndrome (90). Parkinsonian symptoms as well as tics are similarly not (always) characterized by fine and dedicated distal limb movements but rather by broad and general bodily motor symptoms, or stereotypical movements, respectively.

Seen in this light, our results are in agreement with the literature and the evolutionary development of the motor system. In broader strokes, they could be summarized as follows: a first, potentially older motor system is embedded within the agranular prefrontal cortex, projects to midbrain and brainstem motor centers and is responsible for axial movements. Our results suggest that modulating this system would improve axial forms of dystonia such as cervical and truncal phenotypes. A second, "newer" motor system is embedded in the homuncular regions of M1 and, in part, directly projects to spinal cord motor neurons and is involved in distal limb movements such as grasping or single-digit control. Our results suggest that modulating this system would improve appendicular forms of dystonia.

Clinical Implications. At first glance, seemingly inverted optimal stimulation sites for appendicular dystonia/blepharospasm and cervical dystonia might imply a limited performance of subthalamic DBS for generalized manifestations, where both symptom domains are present at the same time. However, this is generally not the case (9, 16) (though see ref. 91), and in our dataset, multiple subjects assigned to both cervical and appendicular groups demonstrated a good response in both components ($N = 8/12$ above 50% improvement, also see Fig. 7 for the representative cases). Indeed, the general electrode trajectory of subthalamic DBS coincides with both optimal target sites that we describe, and both sweet-spots and networks could be engaged to various degrees depending on the symptom profile of any given patient. Since precise surgical targeting of V.o.p. is challenging, employment of directional leads with an extended contact array could be considered. According to the local and structural mapping of symptom improvements, patients with predominantly cervical/axial dystonia would have better outcomes when stimulated at proximal contacts (V.o.p. and adjacent white matter), while appendicular and periocular manifestations would respond better when activating distal contacts (within the STN).

Limitations

The following limitations should be recognized when interpreting our results. First, the study has been conducted on a retrospective dataset composed of two cohorts, with a total of 58 subjects and three groups of dystonia subtypes ranging from 21 to 30 subjects. Importantly, results could not be validated on an additional held-out test set due to the scarce availability of dystonia datasets with STN implantations. Independent retrospective validation or, ideally, prospective trials would be required to confirm our findings. At the same time, robust cross-validation results indicate the potential for the findings to generalize to unseen data. Second, severity of symptoms and their localization are interpreted in the

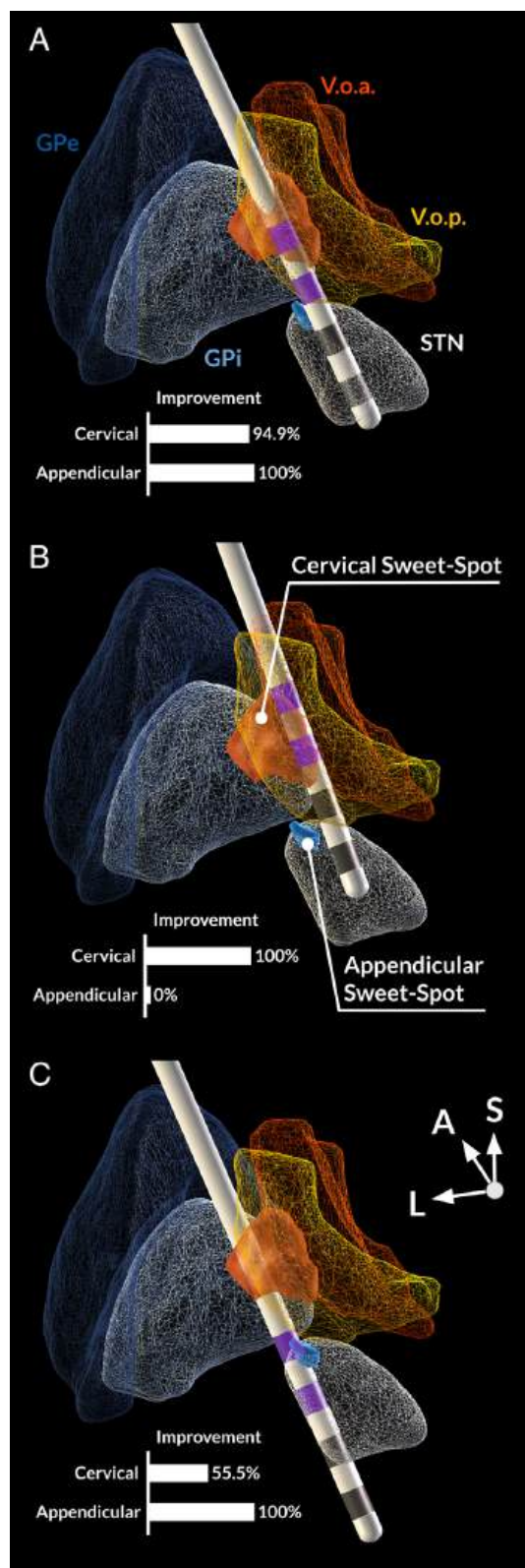


Fig. 7. Three representative cases with dystonia involving multiple body regions. Proximity of active contacts (highlighted in purple) to the sweet-spots (blue—appendicular, orange—cervical) reflects the improvement in the corresponding symptoms. (A) The first patient had improvement in both cervical and appendicular symptom clusters. Their two active contacts mapped to both sweet-spots. (B and C) The second and third patients had strong improvements only in one of the clusters, matching the sweet-spots that were stimulated. Note that the presumably optimal trajectory would coincide with the commonly employed trajectory for DBS in Parkinson's disease.

context of BFMDRS scores, available for both cohorts, while Toronto Western Spasmodic Torticollis Rating Scale (not available for most subjects) could provide additional detail on the cervical component. The BFMDRS scale does not explicitly evaluate hand dystonia, so this subtype (within appendicular dystonia) could not be investigated. Speech and swallowing components could not be comprehensively addressed due to the low number of patients experiencing this symptom at baseline ($N = 12$ with baseline ≥ 3 points).

Third, the acquired patient imaging was of heterogeneous modality and quality. This inherently affects electrode localization accuracy, despite our advanced image processing that includes multispectral nonlinear warping, manual refinement (36), brain shift correction (35) and phantom-validated trajectory reconstruction (37). This limitation also applies to our group-level analysis of electric fields conducted in the common template space based on nonlinear warps of patient scans. Furthermore, for structural and functional connectivity analyses, normative connectomes were employed that do not reflect pathological brain alterations in dystonic patients. Despite using a highly refined anatomical pathway atlas (49), some tracts or their collaterals might be missing, obstructing unequivocal interpretation of the results.

Finally, the DBS effect on the neural tissue was quantified by continuous values of the extracellular electric field magnitude. We deliberately opted for this metric to incorporate a probabilistic impact of the stimulation in our mass-univariate rank-correlation analyses [for more detailed model considerations, see ref. 19]. For more accurate elaboration on white matter recruitment, pathway activation modeling can be employed (92), which, however, requires various assumptions on the axonal morphology and volume conductor complexity.

Conclusions

The potential of subthalamic stimulation for treatment of dystonia has been demonstrated previously (15, 16, 66), and our study now provides neuroimaging evidence underlying improvement and consistency of optimal stimulation sites. Our results demonstrated differential mapping of neural substrates mediating stimulation effects on dystonic symptoms that occur in limbs and eyes vs. cervical/axial presentations. For the former symptoms, effective stimulation directly engaged the subthalamic circuitry, including hyperdirect and indirect pathways. Furthermore, better response for limb dystonia was associated with higher functional connectivity to the corresponding regions in the primary motor cortex. At the same time, improvements of cervical symptoms were associated with more dorsal stimulation of thalamic nuclei and passing fibers, including the cerebellothalamic pathway, with the functional connectivity to the cingulo-opercular network and

cingulate motor regions. Importantly, a precisely placed STN-DBS electrode may engage both of these substrates simultaneously, potentially facilitating alleviation of distributed symptoms. Our results provide a starting point for more deliberate targeting and programming of subthalamic stimulation for different types of dystonia.

Data, Materials, and Software Availability. All anonymized data and code necessary to reproduce the findings of the study are available at OSF (93) and Github (94) repositories, respectively.

ACKNOWLEDGMENTS. B.H. is supported by Einstein Center for Neurosciences Berlin. B.H.B. is supported by the Prof. Dr. Klaus Thiemann Foundation (Parkinson Fellowship 2022). R.L. is supported by BIH Charite Clinician Scientist Program. M.H. is supported by the NINDS Intramural Program. C.G. received honoraria from the Movement Disorder Society for educational activities and academic research support from the Volkswagen Stiftung (Freigeist Fellowship). M.D.F. is supported by grants from the NIH (R01MH113929, R21MH126271, R56AG069086, R21NS123813, R01NS127892, R01MH130666, and UM1NS132358), Neuronetics, the Kaye Family Research Endowment, the Ellison/Baszucki Family Foundation, and the Manley Family. A.H. is supported by the German Research Foundation (Deutsche Forschungsgemeinschaft, 424778381-TRR 295), Deutsches Zentrum für Luft- und Raumfahrt (DynaSti Grant within the EU Joint Programme Neurodegenerative Disease Research, JPND), the NIH (R01 13478451, 1R01NS127892-01, 2R01 MH113929, and UM1NS132358) as well as the New Venture Fund (FFOR Seed Grant).

Author affiliations: ¹Center for Brain Circuit Therapeutics, Department of Neurology, Brigham & Women's Hospital, Harvard Medical School, Boston, MA 02115; ²Department of Neurosurgery, Massachusetts General Hospital, Harvard Medical School, Boston, MA 02114; ³Department of Neurology, Faculty of Medicine, University of Cologne, Cologne 50937, Germany; ⁴Movement Disorders and Neuromodulation Unit, Department of Neurology, Charité—Universitätsmedizin Berlin, Berlin 10117, Germany; ⁵Einstein Center for Neurosciences Berlin, Charité—Universitätsmedizin Berlin, Berlin 10117, Germany; ⁶Berlin School of Mind and Brain, Humboldt—Universität zu Berlin, Berlin 10117, Germany; ⁷Institute of Clinical Neuroscience and Medical Psychology, Medical Faculty University Hospital Düsseldorf, Heinrich Heine University, Düsseldorf 40225, Germany; ⁸Department of Neurology, Center for Movement Disorders and Neuromodulation, Medical Faculty University Hospital Düsseldorf, Heinrich Heine University, Düsseldorf 40225, Germany; ⁹Mallinckrodt Institute of Radiology, Washington University School of Medicine, St. Louis, MO 63110; ¹⁰Department of Neurology, Washington University School of Medicine, St. Louis, MO 63108; ¹¹Department of Biomedical Engineering, Washington University in St. Louis, St. Louis, MO 63130; ¹²Movement Disorder Clinic, Edmond J. Safra Program in Parkinson's Disease, Division of Neurology, University of Toronto, Toronto Western Hospital, Toronto, ON M5T 2S6, Canada; ¹³Human Motor Control Section, Medical Neurology Branch, National Institute of Neurological Disorders and Stroke, NIH, Bethesda, MD 20892; ¹⁴Department of Neurology, Emory University, Atlanta, GA 30322; ¹⁵Department of Neurological Surgery, University of California, San Francisco, CA 94143; ¹⁶Movement Disorders and Neuromodulation Centre, Department of Neurology, University of California, San Francisco, CA 94143; ¹⁷Department of Neurology & Institute of Neurology, Ruijin Hospital, Shanghai Jiaotong University School of Medicine, Shanghai 200025, China; and ¹⁸Department of Neurosurgery, Ruijin Hospital, Shanghai Jiaotong University School of Medicine, Shanghai 200025, China

Author contributions: K.B., T.A.D., B.A.-F., R.L., M.D.F., and A.H. designed research; K.B., C.N., B.H., N.L., S.O., and A.H. performed research; B.H., N.L., S.O., P.A.S., J.L.O., Y.W., C.Z., and A.H. contributed new reagents/analytic tools; K.B., C.N., T.A.D., G.M.M., B.H.B., E.M.G., C.G., M.H., and A.H. analyzed data; C.N., T.A.D., B.H., G.M.M., S.O., B.H.B., E.M.G., N.U.F.D., and J.L.O. edited the paper; R.L., N.U.F.D., C.G., M.H., H.A.J., and Y.W. provided clinical expertise and edited the paper; and K.B., B.A.-F., M.D.F., and A.H. wrote the paper.

1. R. E. Gross, What happened to posteroventral pallidotomy for Parkinson's disease and dystonia? *Neurotherapeutics* **5**, 281–293 (2008).
2. P. Coubes *et al.*, Treatment of early-onset generalized dystonia by chronic bilateral stimulation of the internal globus pallidus. A propos of a case. *Neurochirurgie* **45**, 139–144 (1999).
3. J. K. Krauss, T. Pohle, S. Weber, C. Ozdoba, J. M. Burgunder, Bilateral stimulation of globus pallidus internus for treatment of cervical dystonia. *Lancet Lond. Engl.* **354**, 837–838 (1999).
4. A. Kupsch *et al.*, Pallidal deep-brain stimulation in primary generalized or segmental dystonia. *N. Engl. J. Med.* **355**, 1978–1990 (2006).
5. J. Volkmann *et al.*, Pallidal neurostimulation in patients with medication-refractory cervical dystonia: A randomised, sham-controlled trial. *Lancet Neurol.* **13**, 875–884 (2014).
6. R. Reese, J. Volkmann, Deep brain stimulation for the dystonias: Evidence, knowledge gaps, and practical considerations. *Mov. Disord. Clin. Pract.* **4**, 486–494 (2017).
7. Q. Hao *et al.*, Pallidal deep brain stimulation in primary Meige syndrome: Clinical outcomes and psychiatric features. *J. Neurol. Neurosurg. Psychiatry* **91**, 1343–1348 (2020).
8. J. Volkmann *et al.*, Pallidal deep brain stimulation in patients with primary generalised or segmental dystonia: 5-year follow-up of a randomised trial. *Lancet Neurol.* **11**, 1029–1038 (2012).
9. K. L. Holloway *et al.*, Deep brain stimulation for dystonia: A meta-analysis. *Neuromodulation* **9**, 253–261 (2006).
10. P. Mählkecht *et al.*, Parkinsonian signs in patients with cervical dystonia treated with pallidal deep brain stimulation. *Brain J. Neurol.* **141**, 3023–3034 (2018).
11. C. Schrader *et al.*, GPI-DBS may induce a hypokinetic gait disorder with freezing of gait in patients with dystonia. *Neurology* **77**, 483–488 (2011).
12. S. Meoni *et al.*, Pallidal deep brain stimulation for dystonia: A long term study. *J. Neurol. Neurosurg. Psychiatry* **88**, 960–967 (2017).
13. B. D. Berman, P. A. Starr, W. J. Marks, J. L. Ostrem, Induction of bradykinesia with pallidal deep brain stimulation in patients with cranial-cervical dystonia. *Stereotact. Funct. Neurosurg.* **87**, 37–44 (2009).
14. B. Sun, S. Chen, S. Zhan, W. Le, S. E. Kralh, "Subthalamic nucleus stimulation for primary dystonia and tardive dystonia" in *Operative Neuromodulation: Volume 2: Neural Networks Surgery*, D. E. Sakas, B. A. Simpson, Eds. (Springer, Vienna, Austria, 2007), pp. 207–214, 10.1007/978-3-211-33081-4_23.
15. J. L. Ostrem *et al.*, Subthalamic nucleus deep brain stimulation in primary cervical dystonia. *Neurology* **76**, 870–878 (2011).

16. L. Schjerling *et al.*, A randomized double-blind crossover trial comparing subthalamic and pallidal deep brain stimulation for dystonia. *J. Neurosurg.* **119**, 1537–1545 (2013).
17. A. N. Hock *et al.*, A randomised double-blind controlled study of deep brain stimulation for dystonia in STN or GPi—A long term follow-up after up to 15 years. *Parkinsonism Relat. Disord.* **96**, 74–79 (2022).
18. M. M. Reich *et al.*, Probabilistic mapping of the antidystonic effect of pallidal neurostimulation: A multicentre imaging study. *Brain J. Neurol.* **142**, 1386–1398 (2019).
19. A. Horn *et al.*, Optimal deep brain stimulation sites and networks for cervical vs. generalized dystonia. *Proc. Natl. Acad. Sci. U.S.A.* **119**, e2114985119 (2022).
20. F. Munding, New stereotactic treatment of spasmodic torticollis with a brain stimulation system (author's transl). *Med. Klin.* **72**, 1982–1986 (1977).
21. R. Hassler, T. Riechert, F. Munding, W. Umbach, J. A. Ganglberger, Physiological observations in stereotaxic operations in extrapyramidal motor disturbances. *Brain J. Neurol.* **83**, 337–350 (1960).
22. B. Hollunder *et al.*, Mapping dysfunctional circuits in the frontal cortex using deep brain stimulation. *Nat. Neurosci.* **27**, 573–586 (2024).
23. R. Kaji, K. Bhatia, A. M. Graybiel, Pathogenesis of dystonia: Is it of cerebellar or basal ganglia origin? *J. Neurol. Neurosurg. Psychiatry* **89**, 488–492 (2018).
24. C. Neudorfer *et al.*, Lead-DBS v3.0: Mapping deep brain stimulation effects to local anatomy and global networks. *NeuroImage* **268**, 119862 (2023).
25. D. T. Corp *et al.*, Clinical and structural findings in patients with lesion-induced dystonia: Descriptive and quantitative analysis of published cases. *Neurology* **99**, e1957–e1967 (2022).
26. E. M. Gordon *et al.*, A somato-cognitive action network alternates with effector regions in motor cortex. *Nature* **617**, 351–359 (2023).
27. S. Lin *et al.*, Deep brain stimulation of the globus pallidus internus versus the subthalamic nucleus in isolated dystonia. *J. Neurosurg.* **132**, 721–732 (2020).
28. S. Lin *et al.*, Globus pallidus internus versus subthalamic nucleus deep brain stimulation for isolated dystonia: A 3-year follow-up. *Eur. J. Neurol.* **30**, 2629–2640 (2023).
29. Z. Deng *et al.*, Subthalamic deep brain stimulation in patients with primary dystonia: A ten-year follow-up study. *Parkinsonism Relat. Disord.* **55**, 103–110 (2018).
30. M. S. Lee, C. D. Marsden, Movement disorders following lesions of the thalamus or subthalamic region. *Mov. Disord.* **9**, 493–507 (1994).
31. M. S. LeDoux, K. A. Brady, Secondary cervical dystonia associated with structural lesions of the central nervous system. *Mov. Disord.* **18**, 60–69 (2003).
32. V. K. Neychev, R. E. Gross, S. LeHéry, E. J. Hess, H. A. Jinnah, The functional neuroanatomy of dystonia. *Neurobiol. Dis.* **42**, 185–201 (2011).
33. D. Luzzi, A. F. Gigante, A. Leo, G. DeFazio, The anatomical basis of upper limb dystonia: Lesson from secondary cases. *Neurol. Sci.* **37**, 1393–1398 (2016).
34. D. T. Corp *et al.*, Network localization of cervical dystonia based on causal brain lesions. *Brain J. Neurol.* **142**, 1660–1674 (2019).
35. A. Horn *et al.*, Lead-DBS v2: Towards a comprehensive pipeline for deep brain stimulation imaging. *NeuroImage* **184**, 293–316 (2019).
36. S. Oxenford *et al.*, WarpDrive: Improving spatial normalization using manual refinements. *Med. Image Anal.* **91**, 103041 (2024).
37. A. Husch, M. V. Petersen, P. Gemmar, J. Goncalves, F. Hertel, PaCER—A fully automated method for electrode trajectory and contact reconstruction in deep brain stimulation. *NeuroImage Clin.* **17**, 80–89 (2018).
38. A. Horn, A. A. Kühn, Lead-DBS: A toolbox for deep brain stimulation electrode localizations and visualizations. *NeuroImage* **107**, 127–135 (2015).
39. J. Vorwerk, R. Oostenveld, M. C. Piastra, L. Magyari, C. H. Wolters, The FieldTrip-SimBio pipeline for EEG forward solutions. *Biomed. Eng. Online* **17**, 37 (2018).
40. M. M. Chakravarty, G. Bertrand, C. P. Hodge, A. F. Sadikot, D. L. Collins, The creation of a brain atlas for image guided neurosurgery using serial histological data. *NeuroImage* **30**, 359–376 (2006).
41. S. Ewert *et al.*, Toward defining deep brain stimulation targets in MNI space: A subcortical atlas based on multimodal MRI, histology and structural connectivity. *NeuroImage* **170**, 271–282 (2018).
42. J. B. Ranck, Which elements are excited in electrical stimulation of mammalian central nervous system: A review. *Brain Res.* **98**, 417–440 (1975).
43. L. G. Nowak, J. Bullier, Axons, but not cell bodies, are activated by electrical stimulation in cortical gray matter. Evidence from selective inactivation of cell bodies and axon initial segments. *Exp. Brain Res.* **118**, 489–503 (1998).
44. E. J. Knight *et al.*, Motor and nonmotor circuitry activation induced by subthalamic nucleus deep brain stimulation in patients with Parkinson disease: Intraoperative functional magnetic resonance imaging for deep brain stimulation. *Mayo Clin. Proc.* **90**, 773–785 (2015).
45. A. Horn, M. D. Fox, Opportunities of connectomic neuromodulation. *NeuroImage* **221**, 117180 (2020).
46. N. Li *et al.*, A unified connectomic target for deep brain stimulation in obsessive-compulsive disorder. *Nat. Commun.* **11**, 3364 (2020).
47. A. S. Rios *et al.*, Optimal deep brain stimulation sites and networks for stimulation of the fornix in Alzheimer's disease. *Nat. Commun.* **13**, 7707 (2022).
48. G. M. Meyer *et al.*, Deep brain stimulation for obsessive-compulsive disorder: Optimal stimulation sites. *Biol. Psychiatry* **96**, 101–113 (2023), [10.1016/j.biopsych.2023.12.010](https://doi.org/10.1016/j.biopsych.2023.12.010).
49. M. V. Petersen *et al.*, Holographic reconstruction of axonal pathways in the human brain. *Neuron* **104**, 1056–1063.e3 (2019).
50. B. T. Thomas Yeo *et al.*, The organization of the human cerebral cortex estimated by intrinsic functional connectivity. *J. Neurophysiol.* **106**, 1125–1165 (2011).
51. A. J. Holmes *et al.*, Brain Genomics Superstruct Project initial data release with structural, functional, and behavioral measures. *Sci. Data* **2**, 150031 (2015).
52. A. Horn *et al.*, Connectivity predicts deep brain stimulation outcome in Parkinson disease. *Ann. Neurol.* **82**, 67–78 (2017).
53. R. Hassler, F. Munding, T. Riechert, *Stereotaxis in Parkinson Syndrome* (Springer, Berlin/Heidelberg, Germany, 1979).
54. C. Neudorfer *et al.*, The role of the motor thalamus in deep brain stimulation for essential tremor. *Neurotherapeutics* **21**, e00313 (2024).
55. G. E. Jones, *The Thalamus* (Springer, New York, NY, 1995), vol. 1.
56. N. U. F. Dosenbach, M. Raichle, E. M. Gordon, The brain's cingulo-opercular action-mode network. *PsyArXiv [Preprint]* (2024). <https://osf.io/preprints/psyarxiv/2vt79> (Accessed 12 March 2024).
57. G. Galardi *et al.*, Basal ganglia and thalamo-cortical hypermetabolism in patients with spasmodic torticollis. *Acta Neurol. Scand.* **94**, 172–176 (1996).
58. M. Naumann *et al.*, Imaging the pre- and postsynaptic side of striatal dopaminergic synapses in idiopathic cervical dystonia: A SPECT study using [123I] epidepride and [123I] beta-CIT. *Mov. Disord.* **13**, 319–323 (1998).
59. S. LeHéry, M. A. J. Tijssen, M. Vidailhet, R. Kaji, S. Meunier, The anatomical basis of dystonia: Current view using neuroimaging. *Mov. Disord.* **28**, 944–957 (2013).
60. A. Batla *et al.*, The role of cerebellum in patients with late onset cervical/segmental dystonia? Evidence from the clinic. *Parkinsonism Relat. Disord.* **21**, 1317–1322 (2015).
61. C. Neudorfer, M. Maarouf, Neuroanatomical background and functional considerations for stereotactic interventions in the H fields of Forel. *Brain Struct. Funct.* **223**, 17–30 (2018).
62. K. Butenko *et al.*, Linking profiles of pathway activation with clinical motor improvements—A retrospective computational study. *NeuroImage Clin.* **36**, 103185 (2022).
63. S. Miciocovic *et al.*, Computational analysis of subthalamic nucleus and lenticular fasciculus activation during therapeutic deep brain stimulation. *J. Neurophysiol.* **96**, 1569–1580 (2006).
64. M. A. Khooshnoodi, S. A. Factor, H. A. Jinnah, Secondary blepharospasm associated with structural lesions of the brain. *J. Neurol. Sci.* **331**, 98–101 (2013).
65. S. Jeong, R. Huh, I. Jang, Outcomes of pallidal deep brain stimulation for treating pure blepharospasm. *J. Korean Soc. Stereotact. Funct. Neurosurg.* **18**, 72–80 (2022).
66. C. Kilbane, J. L. Ostrem, Subthalamic nucleus deep brain stimulation for dystonia: Evidence, pros and cons. *Dystonia* **1**, 10609 (2022).
67. H. Xie *et al.*, Deep brain stimulation of the subthalamic nucleus for primary Meige syndrome: Clinical outcomes and predictive factors. *J. Neurosurg.* **140**, 1650–1663 (2024), [10.3171/2023.11.JNS232075](https://doi.org/10.3171/2023.11.JNS232075).
68. S. Horisawa *et al.*, Unilateral pallidothalamic tractotomy at Forel's field H1 for cervical dystonia. *Ann. Clin. Transl. Neurol.* **9**, 478–487 (2022).
69. F. Yin *et al.*, Bilateral subthalamic nucleus deep brain stimulation for refractory isolated cervical dystonia. *Sci. Rep.* **12**, 7678 (2022).
70. C. C. S. Delnoo, J. W. Pasman, C. F. Beckmann, B. P. C. van de Warrenburg, Task-free functional MRI in cervical dystonia reveals multi-network changes that partially normalize with botulinum toxin. *PLoS ONE* **8**, e62877 (2013).
71. E. Sarasso *et al.*, Sensory trick phenomenon in cervical dystonia: A functional MRI study. *J. Neurol.* **267**, 1103–1115 (2020).
72. G. S. Huang, H. Y. Chen, J. C. Tsau, Thalamic hand: A late onset sequela of stroke and its influence on physical function after rehabilitation: Two cases report. *Gaoxiong Yi Xue Ke Xue Za Zhi* **8**, 108–112 (1992).
73. J. Ghika, J. Bogousslavsky, J. Henderson, P. Maeder, F. Regli, The 'jerky dystonic unsteady hand': A delayed motor syndrome in posterior thalamic infarctions. *J. Neurol.* **241**, 537–542 (1994).
74. D. Deleu, M. Lagopoulos, A. Louon, Thalamic hand dystonia: An MRI anatomoclinical study. *Acta Neurol. Belg.* **100**, 237–241 (2000).
75. T. Taira, T. Hori, Stereotactic ventroralis thalamotomy for task-specific focal hand dystonia (writer's cramp). *Stereotact. Funct. Neurosurg.* **80**, 88–91 (2003).
76. S. Horisawa *et al.*, Safety and long-term efficacy of ventro-oral thalamotomy for focal hand dystonia. *Neurology* **92**, e371–e377 (2019).
77. S. Horisawa *et al.*, Magnetic resonance-guided focused ultrasound thalamotomy for focal hand dystonia: A pilot study. *Mov. Disord.* **36**, 1955–1959 (2021).
78. C. N. Prudente *et al.*, A functional magnetic resonance imaging study of head movements in cervical dystonia. *Front. Neurol.* **7**, 201 (2016).
79. M. N. Gallay, D. Jeanmonod, J. Liu, A. Morel, Human pallidothalamic and cerebellothalamic tracts: Anatomical basis for functional stereotactic neurosurgery. *Brain Struct. Funct.* **212**, 443–463 (2008).
80. A. Scerrati *et al.*, Thalamic ventral-oralis complex/rostral zona incerta deep brain stimulation for midline tremor. *J. Neurol.* **271**, 6628–6638 (2024).
81. S. Horisawa *et al.*, Deep brain stimulation of the Forel's field for dystonia: Preliminary results. *Front. Hum. Neurosci.* **15**, 768057 (2021).
82. V. E. Rozanski *et al.*, The role of the pallidothalamic fibre tracts in deep brain stimulation for dystonia: A diffusion MRI tractography study. *Hum. Brain Mapp.* **38**, 1224–1232 (2017).
83. A. J. Blood *et al.*, Evidence for altered basal ganglia-brainstem connections in cervical dystonia. *PLoS ONE* **7**, e31654 (2012).
84. H. G. J. M. Kuypers, "Anatomy of the descending pathways" in *Comprehensive Physiology* (John Wiley and Sons Ltd., 2011), pp. 597–666, [10.1002/cphy.cp10213](https://doi.org/10.1002/cphy.cp10213).
85. R. N. Lemon, Descending pathways in motor control. *Annu. Rev. Neurosci.* **31**, 195–218 (2008).
86. L. C. Triarhou, The Economo-Koskinas atlas revisited: Cytoarchitectonics and functional context. *Stereotact. Funct. Neurosurg.* **85**, 195–203 (2007).
87. R. J. Nieuwenhuis, C. H. Voogd, *The Human Central Nervous System* (Steinkopff, Heidelberg, Germany, 2007).
88. C. B. D'Andrea *et al.*, Substructure of the brain's cingulo-opercular network. *bioRxiv [Preprint]* (2023). <https://doi.org/10.1101/2023.10.10.561772> (Accessed 12 March 2024).
89. J. Ren *et al.*, The somato-cognitive action network links diverse neuromodulatory targets for Parkinson's disease. *bioRxiv [Preprint]* (2023). <https://doi.org/10.1101/2023.12.12.571023> (Accessed 12 March 2024).
90. J. C. Baldermann *et al.*, A critical role of action-related functional networks in Gilles de la Tourette syndrome. *Nat. Commun.* **15**, 10687 (2024), <https://doi.org/10.1038/s41467-024-05100-0>.
91. H. Fan *et al.*, Deep brain stimulation treating dystonia: A systematic review of targets, body distributions and etiology classifications. *Front. Hum. Neurosci.* **15**, 757579 (2021).
92. K. Gunalan *et al.*, Creating and parameterizing patient-specific deep brain stimulation pathway-activation models using the hyperdirect pathway as an example. *PLoS ONE* **12**, e0176132 (2017).
93. K. Butenko *et al.*, Engaging dystonia networks with subthalamic stimulation. *OSF*. https://osf.io/zhtjk/?view_only=c204b212c9a04852b3c316f1e05013c. Deposited 12 November 2024.
94. K. Butenko *et al.*, Engaging dystonia networks with subthalamic stimulation. *GitHub*. https://github.com/Kinway25/leaddbs/tree/STN_DBS_DYT. Deposited 29 October 2024.